SPACE
SCIENCES
LABORATORY

N71-34370

CASE FILE
COPY

A SUPERCONDUCTING MAGNETIC SPECTROMETER
FOR COSMIC RAY NUCLEI

L. H. Smith and A. Buffington
Space Sciences Laboratory,
University of California, Berkeley, California

and

M. A. Wahlig and P. Dauber
Lawrence Radiation Laboratory,
Berkeley, California

July 1971

Space Sciences Laboratory Series 12 Issue 47

UNIVERSITY OF CALIFORNIA, BERKELEY

Space Sciences Laboratory
University of California
Berkeley, California   94720

A SUPERCONDUCTING MAGNETIC SPECTROMETER FOR COSMIC RAY NUCLEI

L. H. Smith and A. Buffington
Space Sciences Laboratory,
University of California, Berkeley, California

and

M. A. Wahlig and P. Dauber
Lawrence Radiation Laboratory, Berkeley, California

July 1971

Space Sciences Laboratory Series 12 Issue 47

A Superconducting Magnetic Spectrometer for Cosmic Ray Nuclei*

L. H. SMITH AND A. BUFFINGTON
Space Sciences Laboratory,
University of California, Berkeley, California

and

M. A. WAHLIG AND P. DAUBER**
Lawrence Radiation Laboratory, Berkeley, California

ABSTRACT

This paper describes the design, calibration, and operation

of a magnetic spectrometer for particle astronomy. The

spectrometer consists of a cryogenic magnet, optical spark

chambers, scintillation detectors, and associated elec-

tronics. The instrument has been flown in a balloon

gondola to 4.8 grams/cm^2 residual atmosphere, where it

was used to analyze the charge and differential rigidity

spectra of primary nuclei from 5 to 100 GV/c.

INTRODUCTION

For many years, the energy of cosmic ray particles has been measured using calorimetric techniques. In such experiments a particle deposits its energy in a detector with alternating scintillator and absorber layers, and the emitted light in the scintillators is measured. Good energy resolution can be obtained with this technique, provided that a large fraction of the particle energy is deposited in the sensitive portion of the calorimeter. However, very heavy absorbers between the sensitive layers are required to measure high energy nuclear cosmic rays, resulting usually in approximately 25 percent energy resolution, combined with the disadvantage of a very heavy experimental package.

Terrestrial experiments have used magnetic spectrometers for a long time, but these conventional magnet systems were very heavy and required sustained power, and thus were impractical for balloon experiments.

By 1963, practical magnetic spectrometers could be made with super-conducting magnets. At this time Luis Alvarez suggested that, since light-weight magnetic spectrometers were feasible, they could be applied to high-energy cosmic ray experiments. Furthermore, this technique would provide a unique means of measuring the sign of the charge of the cosmic ray particles, thus permitting separation of electrons from positrons and of matter from anti-matter. Since that time, several small permanent magnetic spectrometers for balloon-borne cosmic ray experiments have been described in the literature.[1,2]

The following text describes a spectrometer which uses a single coil to make a small superconducting magnet (SSCM). The spectrometer utilizes four sets of optically viewed spark chambers to define the particle

trajectory in the magnetic field. The chambers are triggered by a three-
fold coincidence from three plastic scintillators. The pulse heights from
these scintillators and from a pair of cesium iodide crystals are used to
determine the charge of the particle. The pulse height data are digit-
ized and displayed on a light panel photographed by the spark chamber
cameras. An automatic measuring machine measures the 60,000 photographs
accumulated during an experiment.

A balloon flight of this apparatus was made on September 18, 1970,
to measure the spectra of cosmic ray nuclei with charges ranging from
protons to iron. A search for anti-nuclei events was made in these data.
The physics results from this flight will be reported elsewhere. The con-
figuration chosen for this flight had a geometry factor of 660 cm^2 sr
with an average line integral of 5 kG-m. However, care must be used in
employing these specifications because the rigidity (p/Z) resolution
varied over the surface of the detectors due to the non-uniform magnetic
field. A knowledge of the characteristics of the instrument will be
helpful to readers critically evaluating our results; a description of
these characteristics is the object of this article.

OVERALL DESCRIPTION OF THE INSTRUMENT

The superconducting magnetic spectrometer was designed to analyze
the rigidity of particles up to 100 GV/c. This design figure was based
upon a current of 100 amp in the magnet and an overall accuracy of
±0.2 mm in the location of the trajectory in each of the four spark
chambers.

The momentum of each particle was determined by measuring the loca-
tion of the trajectory with optical spark chambers at two planes 25 cm

apart above the magnet, and again at two planes below. Therefore, the trajectory had three constraints allowing a goodness-of-fit to be calculated for the momentum of each particle. The magnetic field at any point along the trajectory was computed using a superposition of 48 simple current loops approximating the coil geometry. Checks by "mapping" the actual field of the magnet showed the line integral was calculated by this technique correct to within a few percent for any trajectory.

Figure 1 shows the 24-inch-diameter magnet, centrally located in a spherical aluminum shell housing the experimental apparatus. The coil was placed along a diagonal of the spark chambers so that the light pipes of the detectors on either side of the magnet could be kept out of the spark chamber mirrors' optical path. These scintillation detectors beside the magnet (S_2 left and S_2 right), along with one 75 cm above the magnet center (S_1) and another 75 cm below (S_3), provided a coincidence trigger for the spark chambers. Anticoincidence detectors on either side of the magnet could be used to eliminate triggering on those events which had particles passing through the magnet. The trigger rate on particles of charge three and greater was about eight times higher when the anti-detector was not included in the trigger criterion. Examination of these events showed they were mainly due to secondary particles operating the trigger counters.

All the photomultiplier tubes viewing the detectors were located near the periphery of the gondola, where the magnetic field was lowest. The axis of each tube was placed nearly perpendicular to the magnetic flux to facilitate the shielding operation. Adiabatic light pipes carried the scintillation light from the detectors to the photomultiplier

tubes. Pulse height analysis was performed on the photomultiplier output signals, using linear gate circuits plus analog-to-digital converters.

The mirror system viewing the spark chambers occupied two sides of the supporting frame, and the optical path to the cameras passed along the other two sides. The spark gaps for triggering the spark chambers were located on one side of the frame not occupied by the mirrors; the helium reservoir was on the remaining side. Two redundant high-speed electronic systems, which performed the detector logic, were located beneath the gondola frame along with the power supplies and digital data processing system.

The liquid helium supply and vent system for the magnet extended on two tubes out beyond the main frame and then passed up through the gondola shell. The boil-off stack allowed the helium gas to vent through two absolute pressure relief valves to the outside. Liquid helium could also be added to the reservoir through the vent stack after the shell was placed on the apparatus. The gondola could therefore be closed and the magnet be charged, and the experiment could remain in a flight-ready condition for many days. The expendables, such as spark chamber gas, could be supplied from outside through fittings in the equatorial flange just before launch.

Prior to flight, the gondola shell was purged with dry nitrogen gas and then sealed to maintain a constant gas density. A nitrogen gas make-up system would have provided more gas at the rate of 12 cubic feet per hour in the event a leak in the shell had occurred.

The radio command and telemetry system was hung below the gondola in order to facilitate access after the gondola shell was closed, and also to escape the more intense magnetic field. The telemetry provided

a continuous real-time monitor of command states, housekeeping data, detector counting rates, digital bit strings with pulse height data, camera operation, and a Loran C repeater. Redundant parallel channels in both telemetry and command receivers insured control of the experiment. Housekeeping channels recorded various temperatures, pressures, and voltages, so any potential malfunctions could be detected and the flight profile be altered accordingly. The vital portions of the electronics system were designed with parallel redundancy, so if a malfunction were detected using the housekeeping or physics telemetry, the bad system could be turned off and the alternate system commanded into operation.

Table I gives a list of the specifications for our apparatus. The overall weight was 4,000 pounds, including balloon control electronics. A flight with this gondola was made to 4.8 g/cm^2 residual altitude with a 20-M-cubic-foot balloon. The altitude was a good match to the material in the gondola (6.9 g/cm^2). After data-taking was complete, the balloon was valved down to an 80,000-foot altitude. Then the gondola payload was released onto its parachute and recovered having suffered only minor damage in the landing.

SPECTROMETER

Magnet

Generally speaking, the design criterion for the magnet was a maximization of the line integral-geometry factor (kilogauss-meters-square centimeters-steradians) with a 2-foot-diameter, 400-pound magnet and cryostat. Helmholtz coils were investigated first. Pairs of coils, however, have the decided disadvantage that a supporting structure would be necessary to keep the coils apart. A support structure between the coils would complicate the design by its need to protrude through the

vacuum walls. Hence, the cryostat would have to be built over the entire assembly and this would increase the weight. Furthermore the Helmholtz configuration would not use the field outside the coil pair and thus seemed wasteful. For these reasons, we elected to utilize both sides of a single coil in order to get a maximum line integral-geometry factor for a fixed weight.

Niobium-titanium superconducting wire with copper cladding was used for the coil. This wire had a unique oxide insulation developed by Super-Magnetics.[3] The thin oxide insulation allowed better cooling of the wire by the liquid helium than would conventional insulation. Furthermore, it permitted the wire to be more densely packed on the coil. The wire had a 30-mil OD and a 15-mil core of niobium-titanium. A short sample of the wire sustained 150 amp at liquid helium temperature in a 60-kG field.

The wire was wound on an aluminum coil form, which was perforated with holes and milled with grooves to allow the liquid to get to the wire coil, and to aid the helium gas in its escape. The coil form was a spool with 3/8-inch walls having a 12-inch ID, 24-inch OD, and 2-1/2-inch-wide wire space. This aspect ratio was chosen because it gave a maximum average line integral over a 7- by 20-inch area beside it. The wire was wound 12,800 turns on the spool with fiberglas cloth between each 75-turn layer. In principle, this coil could be charged to 108 amp before the innermost turns of wire would exceed their short sample limit. The magnet was once charged to 105 amp before it transitioned, but typically we charged it to only 100 amp. Operational difficulties in charging the magnet for our flight caused us to compromise on our design specification for the data-taking, and fly the magnet charged only to 70 amp.

Figure 2 shows the line-integral provided by the single coil when charged to 100 amp, when a 7- by 20-inch area on each side of the magnet is used. For experiments where a smaller geometry factor could be tolerated, as when measuring the proton spectrum, the usable area could be reduced to give a higher average line-integral. For example, using a geometry factor of only 20 cm^2 sr, we could obtain our capacity of 60,000 proton triggers in a 10-hour flight, and the average line integral would be increased to 8.5 kG-m. (This assumes a proton integral flux of 0.08 events per cm^2 sr sec above a 4.6 GV/c geomagnetic cutoff.)

The magnet was charged through two 10-foot leads of 1/4-inch copper tubing. These were spiraled around in the boil-off stack, thus offering a large cooling area for the boil-off gas. These leads were connected in parallel with a small coil of superconductor called the "persistency switch." During the charging operation the persistency switch was kept "normal" (not superconducting) by heating a nichrome wire threaded between the turns of the superconductor. When an external voltage, V, was applied to the charge leads, the switch conducted very little current and the magnet accepted current at the rate $dI/dt = V/L$, where the inductance, L, was about 65 henries. When the desired current in the magnet was reached, the charging voltage was reduced until zero voltage was left across the persistency switch. The external power supply still had a voltage on it due to the charge-line resistance. The switch heater was then turned off and the liquid helium cooled the switch, making it superconducting. Finally, the external supply was switched off, forcing the magnet current through the switch. Shunted by this switch, the magnet has run for over a week without detectable loss of current.

Cryostat

The magnet cryostat was designed so the field on both sides of the coil could be utilized. Furthermore, the vacuum space and wall thickness around the magnet were minimized to make the usable area close to the wire. Figure 3 shows the result of this design. Since only about 10 liters of helium were contained around the magnet, a reservoir was necessary elsewhere to provide the capacity for a 10-hour flight. The total liquid capacity was 45 liters, which lasted 16 hours with our boil-off rate. A connecting tube at the bottom of the magnet provided for liquid flow, and another tube at the top allowed boil-off gas to escape. The two charge leads from the magnet went through the lower tube to the persistency switch located beneath the reservoir.

The coil form and magnet helium flask were fabricated from aluminum for good heat conduction. The remainder of the helium flask including the reservoir and boil-off tube were made of stainless steel to minimize the heat loss through the tube. Two vacuum-brazed joints were used at the magnet end of the cross tubes to join the aluminum and stainless portions of the helium flask. All joints in the inner flask were welded or soldered except for a copper gasket located at the top of the boil-off tube.

About 65 layers of "superinsulation" were wrapped around the helium flask (inner vacuum wall) to reduce radiative heat loss. Each layer consisted of a 1/4-mil mylar sheet, aluminized on both sides, and a sheet of nylon bridal net. The nylon bridal net prevented layer-to-layer heat shorts because it touched the aluminized mylar only at the thread intersections. Slits were cut in the mylar to let gas escape to aid evacuation. A vacuum of 10^{-4} Torr or less was required for adequate insulation;

however, once liquid helium was put in the flask, the vacuum space was quickly cryopumped so that 10^{-5} Torr or less was typical.

When a vacuum of 10^{-4} Torr or less was reached in the vacuum space, the magnet could be cooled. Prior to cooling the magnet, all condensable contaminates were removed from the helium flask by pumping on it for several hours. In particular, it was important to remove moisture from the wire's hygroscopic insulation. Then the flask was back-filled with dry nitrogen gas, and liquid nitrogen was transferred to pre-cool the magnet. Several hours of soaking brought the magnet to 80 °K, whereupon the liquid nitrogen was removed and the flask was again evacuated to remove all nitrogen. After back-filling the magnet space with dry helium gas, liquid helium could be transferred into the flask. A 3- or 4-hour soak was required to bring the magnet to 4.2 °K before it could be charged. The magnet could remain charged even when the helium reservoir was almost empty and only 13 inches of liquid remained in the magnet flask. The magnet could be operated for 11 hours on one filling. After this time it either had to be turned off or the helium replenished, to prevent a transition.

Electronics and Telemetry

Figure 4 shows a schematic diagram of the trigger electronic system. A trigger was permitted only when coincident pulses occurred for all three of the trigger scintillators S_1, (S_2 left or S_2 right), and S_3. Attenuators between photomultipliers and discriminators in each of these trigger inputs enabled us to select trigger thresholds by ground command. We had the options of triggering on a minimum charge on one, two, or three. In addition, we had command control over the anticoincidence

scintillator, which could be included or excluded from the trigger criterion. A gate generator in each trigger system imposed a dead time between triggers to allow time for the cameras to photograph the spark chambers, data board, fiducial lights, and a clock, and then advance the film. The dead time for our flight was set at 218 msec.

The particle's time of flight in passing between detectors S_1 and S_3 was measured by a time-to-analog converter, followed by an analog-to-digital converter for data board display. This measurement provided a rejection of events in which an albedo (incident from below) particle might simulate an anti-matter (negatively charged) event. The 10-nanosec timing difference between these two types of events was sufficiently greater than the 4-nanosec half-width of the timing distribution for normally incident particles, so that we had 99 percent rejection against albedo events.

Redundancy played a major role in our electronics design. We had two complete electronic trigger systems, either one of which was capable of proper data-taking. The telemetry provided a monitor of trigger rates for each trigger system, both before and after the action of the gate (dead time) generator. Ground-controlled switching provided separate control over each trigger system. The singles rates of each scintillator were also telemetered through a slow sampling circuit. We had separate radio control over individual phototubes. If the trigger or singles rates indicated a faulty phototube, we could command it OFF. The S_1 and S_3 detectors each had two photomultiplier tubes with their output pulses added, so commanding one OFF would merely have changed the threshold. Commanding OFF one of the S_2 photomultipliers would have reduced the geometry factor by one-half but left the thresholds unchanged. In any case, a total failure would have been avoided.

Power for the gondola was supplied by four battery packs. Two sets of Silvercels,[4] containing 200 amp-h each at 28 V, supplied power to the constant-current portion of the electronics. Two other packs of 100 amp-h cells provided the power for the pulsed systems, such as cameras, spark chamber power supplies, and data board lights. Six hundred watts total were dissipated during our flight. The redundancy concept of design was extended to the battery hook-up so the failure of any single battery pack would not result in total loss of data.

Table II shows the normal triggering rates at altitude for the various trigger modes. In each case, the gated triggering rates were what one would expect from the ungated triggering rate and the 218 msec dead time. A scan of the events after the flight showed that about half of the triggers were good events, for the data taken with the anticoincidence scintillator in the trigger criterion. Almost all the extra triggers added by excluding the anticoincidence had various background topologies.

For the trigger logic units, we selected several standard NIM-style circuits which met our specifications for magnetic insensitivity, low power drain, and good thermal performance. Most of the units had to be modified to provide better spark chamber noise suppression.

Spark Chambers

The optical spark chamber areas and gap spacings are given in Table I. The 1/4-inch-thick plates were constructed from polyurethane foam with 0.004-inch-thick aluminum foil glued to both sides. Parallel plate glass was used for the spark chamber windows. A module consisted of a high voltage plate with a ground plate on each side. Gas inlet and outlet ports were located on opposite corners of each spark chamber gap for a continuous

flow of neon-helium gas. Each of the four spark chambers consisted of a pair of modules put together with a wedge-shaped piece of Textolite so the camera could view through to the rear of each module. Four such spark chambers (16 gaps total) were used to define the particle trajectory as it traversed the magnetic field.

A gas mixture of 90 percent neon and 10 percent helium flowed continuously through the spark chambers at the rate of 0.5 cu ft/h. The flow was controlled by a pair of ±0.2 psi pressure transducers actuating a pair of solenoid valves. The differential spark chamber pressure was maintained between 0.3 and 0.5 mm Hg. The use of redundant transducers and valves prevented a single failure from being able to rupture the chambers.

Figure 5 shows the redundant scheme used to power the spark chambers. Alternate modules were pulsed by different spark gaps which were, in turn, supplied by separate power supplies, which were, in turn, supplied by separate batteries. Should a single failure have occurred, the worst consequence would have been the loss of half of the spark chamber gaps, and the rigidity resolution would have become worse by a factor of $\sqrt{2}$, but the experiment would not have been a total failure.

When the trigger electronics had made a decision to trigger, it sent two 0.7-V logic-level trigger pulses to the trigger inputs for the spark chambers. Here each trigger pulse was amplified to about 1 kV by a Marx generator employing avalanche transistors. Then a spark gap with a barium titanate trigger electrode amplified the pulse to 9 kV. Finally, these low-power, 9-kV pulses were applied to the four slave spark gaps, which applied 10-kV pulses to each of the spark chamber gaps. A dry nitrogen atmosphere was maintained in all spark gaps because our experience

has shown this procedure lengthens the life of the electrodes by a factor of 2. Several million pulses were obtained between gap cleanings; little effect on spark chamber firing efficiency was observed during this life-time. The nitrogen atmosphere also increased the range of high voltage allowable on the gaps between spontaneous breakdown and poor triggering, all at a constant trigger voltage.

Optical System and Cameras

The mirror system folded the two 90-degree stereo views from each of the four spark chambers to one corner of the gondola frame. Two 35-mm cameras simultaneously viewed the chambers along with a data board. One hundred and twenty lights on this data board indicated the pulse heights in each detector, the particle time of flight, event number, and various command states involving the trigger criterion.

Twenty-two mirrors were used to view the chambers. However, the light from a given spark reflected off only five of these mirrors on its path to the cameras. The larger mirrors were made from half-inch plate glass backed with a 2-inch-thick glass foam to give them stiffness. Each mirror was mounted using a three-point adjustable support system. A fiducial frame placed around the spark chambers supported the fiducial lights which appeared in each picture. These lights provided the local frame of coordinates for measurement of the sparks in each view of each chamber. When the experiment was first assembled, the relation between these lights was carefully recorded, so we could use them to reconstruct the spark locations into a common coordinate frame for all the spark chambers, and then relate the magnet coil position to this same frame. In the data analysis, straight-track events recorded with the magnet

turned off provided small corrections to take account of changes in the fiducial frame that might have occurred since its original assembly. In addition to the fiducial lights, this frame also held several rows of regularly spaced calibration grid lights for each chamber. These calibration grids operated at regular intervals (once every 1024 frames) during the data-taking and provided a continuing calibration of distortions in the mirrors.

The mirrors were aligned before flight using three small lights centrally mounted behind small holes in each rear fiducial frame panel and shining through a hole in the front panel. These three lights were observed at the two camera positions and at a viewing port between the cameras. A small misalignment in any mirror would move the light out of view of the observing port in the gondola shell flange. In this way a visual check of the optical system was made just prior to launching the gondola. During flight, these lights were turned on during the calibration grid pictures and provided a continuous check on the optical alignment.

Pictures of the spark chambers and data board were taken with a pair of 35-mm Traid[5] cameras, which were extensively modified by us. Each camera had a nominal thousand-foot magazine into which we put 2,000 feet of 2.5-mil mylar base film (Eastman No. SO-235). The resulting capacity was approximately 30,000 frames per camera. The advance of both cameras was monitored by telemetry to check for double framing or other signs of failure. Each camera could be commanded ON or OFF independently of the other. The sparks in the chambers were instantly recorded by the open shutter camera, then the fiducial lights, data board lights, and clock lights were illuminated; and finally, the camera was advanced. The total time for these operations was about 200 msec.

Each camera independently viewed both stereo views of the spark chambers, as well as the data box and fiducial lights. Under normal data-taking operation, only one camera at a time was in operation, allowing the recording of a maximum of 60,000 events. A failure of one camera would only have resulted in a reduced number of events recorded.

Performance of the Spectrometer

The spectrometer performed almost flawlessly during flight. The only difficulty arose when one of the gate generators began operating erratically. This failure gave indications in several telemetry channels and we remedied it promptly by switching to the parallel logic system.

When the gondola was recovered and the film developed, we began our data analysis sequence. The data events were automatically measured using the LRL SASS measuring instrument.[6] Magnet-off straight-track events were reconstructed and fit to straight lines in our analysis sequence. A least-squares fitting routine used the events to solve for nineteen parameters describing the important components of uncertainty in our fiducial frame survey. The scanners also hand-measured several of our calibration grid pictures from each camera; these were averaged and used to generate a correction routine which took out the distortions in the spark chamber optics mirrors. The calibrations were then incorporated into our reconstruction program and applied to all of the data. Internal consistency of these calibrations showed that our ability to reconstruct the location of a four-spark segment within a single chamber was accurate to ± 0.14 mm in real space.

Other sources of error were the physical jitter of the sparks and the measurement error. To investigate this, we used events whose charge

was uniquely determined by the recorded scintillator pulse heights. The four-spark segments of the events were fit to a straight line and the standard deviation calculated. The distribution of standard deviations for each charge had the correct shape for a gaussian jitter distribution of the sparks around the true track. Figure 6 shows the distribution of helium nuclei. The long tail is commonly seen in spark chamber studies of this sort. It is thought to be a result of delta-ray activity in the spark chamber gaps.[7] If the spark jitter is a result of diffusion of the tracks's ion pairs before the high voltage is placed on the spark chamber, it should diminish with increasing ionization. In fact, for our spark chambers, the observed jitter mean values ranged from ±0.2 mm for proton tracks to less than ±0.12 mm for carbon tracks.

A magnetic spectrometer actually measures the bend angle of the particle under analysis. In first order, this bend angle is proportional to the "specific curvature" (inverse rigidity) of the particle. The error in specific curvature is approximately constant over the range of rigidity measured in our balloon flight. To determine the resolution of the spectrometer, we analyzed a large sample of magnet-off straight-track events as though they were curved-track events. These events were obtained with the triggering threshold for $Z \geq 2$. A cut on the goodness-of-fit parameter for the data rejected most of the low momentum (atmospheric secondaries) or interaction events at the expense of no more than 5 percent of the good straight-throughs. Figure 7 shows the resulting distribution of specific curvature. The characteristic width of the distribution corresponds to a spectrometer resolution of ±0.0165 (c/GV) or a maximum resolvable rigidity of 60 GV/c. Monte Carlo studies with our momentum analysis program showed this resolution could be

explained by multiple scattering, plus the errors mentioned above. The unfolding of the multiple scattering contributions showed that, for high momentum events where the multiple scattering is negligible, the maximum resolvable momentum of our instrument is 85 GV/c. However, the worse spark jitter contribution for protons makes the resolution for protons worse by a factor of approximately $\sqrt{2}$.

How well did this performance agree with the design specifications? The original design figure of a maximum detectable momentum (MDM) of 100 GV/c was based upon a current of 100 amp in the magnet and a spark chamber accuracy of 0.2 mm. We flew with only 70 amp in the magnet but achieved a spatial accuracy of 0.16 mm, resulting in our experimental MDM of 85 GV/c.

CHARGE MEASURING SYSTEM

Detectors

The spark chamber trigger pulse also initiated a pulse height analysis system that recorded the pulse heights from the S_1 and S_3 plastic trigger scintillators. In addition, it analyzed the pulses from a pair of cesium iodide (sodium-doped) crystals placed just above the S_2 scintillators, as shown in Figure 3. Each cesium iodide detector was a mosaic of four 5- by 7-inch by 1/8-inch-thick crystals. The pieces were immersed in a silicone oil with a high index of refraction, and glued into a lucite box of total thickness 9/16 inch. The box was wrapped with aluminum foil and black tape, as for a plastic scintillator, and viewed through an adiabatic light pipe.

With the spark chamber information available, one could in principle correct even the most nonuniform scintillator for positional dependence

of pulse height. However, it was advantageous to reduce the positional

dependence to a minimum. In S_1 and S_3 this was accomplished by viewing

each scintillator with a pair of phototubes through long adiabatic

light pipes from opposite ends. The pulses from the pair of tubes on

each scintillator were added and the sum was then split to go to the

trigger system electronics and to the pulse height analysis electronics.

The detectors were "mapped" using a beam of π-mesons from the Berkeley

Bevatron accelerator, measuring the pulse heights produced at different

areas over the surface of the counter. A spatial nonuniformity of only

5 percent was obtained by this system. For the cesium iodide detectors,

which were each viewed by only a single phototube, we found an end-to-end

variation in pulse height of 35 percent. One can compare this with an

end-to-end variation of 20 percent for a plastic scintillator of compar-

able dimensions.

Electronics

The photomultiplier tubes were made to have adequate dynamic range

to observe nuclei of charge one to twenty-six. A tapered resistor

divider string was used with the photomultipliers to prevent space

charge saturation of the final dynodes. To obtain more easily the

dynamic range needed, pulses from both the anode and next-to-last dynode

were used by the pulse height analysis electronics. Before we achieved

our specification (a pulse height analysis system with a dynamic range

of 500 and 1/2 percent temperature stability from 0 °C to 60 °C), we had

to perform extensive modifications on the commercial linear gates.

The electronic response to light in the scintillator was not linear,

due to some saturation in the analog-to-digital converter. This effect

did not reduce the charge resolution, however, because it proportionally

narrowed both the pulse height distributions and the spacing in pulse height between neighboring elements. Moreover, we had a consistency check for elements between charge three and ten, since these data appeared on-scale in both the anode and dynode pulse height analysis channels. Each channel was divided into 1024 bins.

The photomultiplier pulses ranged linear in amplitude from several millivolts to 1 volt. After the pulses were gated in the linear gate system and digitized in the analog-to-digital converters, the results were read into a digital scanner. This unit buffered the digital bits from the pulse height analysis units together with the time-of-flight measurement result, the frame number, and the various other information to be displayed on the data board. After the data board lights were flashed, the information was strobed from the buffer, converted into a serialized bit string, and telemetered to the ground for our real-time analysis.

Resolution of the Charge Measuring System

The final resolution of a charge measuring system is set by statistical fluctuations in the collected photoelectrons of the viewing system, by Landau fluctuations in the energy deposition, by saturation in the scintillation mechanism,[8] and by residual error in the spatial and angular corrections to the pulse height. The cesium iodide scintillators also had the property that their light output was temperature-sensitive.[9] To meet this final difficulty, we monitored the temperature of the cesium iodide crystals throughout the flight with several of the housekeeping telemetry channels. This correction did not prove to be necessary, however, since the temperature of the crystals varied during the data-taking by only 2 °C.

The spark chamber information was used to reduce the variation from spatial and angular effects to a negligible level. The effect on resolution due to statistical fluctuations in photoelectrons was about $\Delta Z = \pm 0.4$ for the plastic scintillators, and ± 0.2 for the cesium iodide detectors. Here, by ΔZ we mean the half width of the pulse height distributions, normalized to the spacing between elements. The combined pulse heights from our three detectors improved the charge resolution giving approximately $\Delta Z = \pm 0.15$.

We employed cesium iodide in our apparatus in an attempt to distinguish better the highly ionizing particles. Saturation sets in at much larger ionization for the cesium iodide than it does for the plastic scintillator. However, our data showed that saturation in the scintillator was not an important effect as far as charge resolution was concerned until we were measuring elements above neon.

The pulse height distribution for some of our $Z \geq 3$ data appears in Figure 8. The three counters have been averaged together and all corrections applied. Analysis of the data in Figure 8 shows that our resulting Z resolution is ± 0.15 charges, and that there is a very small (less than 4%) overlap between equal-abundance neighboring elements. This resolution is what we would expect from our sources of uncertainty described above.

SUMMARY AND ACKNOWLEDGMENTS

We believe the superconducting magnetic spectrometer technique can now be considered practical for balloon experiments. Many new experiments, which were formerly impossible, can now be made; for example, the separate measurement of high energy electron and positron cosmic

ray spectra, the search for anti-matter in the cosmic rays, and the separation of cosmic ray isotopes. Physicists have been restricted in their information about the galactic cosmic rays due to uncertainties in the solar modulation at low energies, and by technique at high energies. The magnetic spectrometer extends the range of measurable energies by one or two orders of magnitude.

We anticipate flying the present spectrometer again with minor changes to gain better statistics on beryllium-to-iron data. In addition, we intend a high-statistics flight on helium alone to search for anti-nuclei.

The successful design, testing, and flight of this gondola would not have been possible without the skill and perseverance of the many members of our group. We would like especially to acknowledge the work of Jack Lloyd, who designed the superconducting coil and contributed many valuable ideas to the rest of the gondola design. Our flight took place out of the National Science Foundation-supported National Center for Atmospheric Research launch facility at Palestine, Texas. We would like to thank the Palestine launch crew for the kind hospitality extended to us during our operations there. Finally, we would like to thank Luis W. Alvarez for his continuing interest and support throughout this experiment.

REFERENCES

[1] James A. DeShong, Jr., Robert E. Daniels, Roger H. Hilderbrand and Peter Meyer, *Rev. Sci. Ins.* 35, 1035 (1964).

[2] Yash Pal; private communication.

[3] Super-Magnetics, 1607 Lynwood Drive, Concord, California 94521

[4] Silvercels, Yardney Electric Corporation, 40-52 Leonard St., New York 13, N.Y.

[5] Traid Corporation, 777 Flower Street, Glendale, California, 91201

[6] Donald H. Zurlinden, SASS (Spark Chamber Automatic Scanning System), Report No. UCRL-17695, Lawrence Radiation Laboratory, Berkeley, University of California, (July 1967) (unpublished); *Datamation*, March 1970.

[7] W. A. Wenzel, "Spark Chambers", Report No. UCRL-11319, Lawrence Radiation Laboratory, Berkeley, University of California (1964).

[8] G. D. Badhwar, C. L. Deney, B. R. Dennis, and M. F. Kaplon, "The Non-Linear Response of the Plastic Scintillater NE 102," *Nucl. Inst. Meth.* 57, 116 (1967;

J. F. Ormes, M.S. Thesis, Univ. of Minn. (1965) unpublished;

T. T. von Rosenvinge, private communication.

[9] J. Menefee, Y. Cho, C. Swinehart, "Sodium-Activated Cessium Iodide as a Gamma - Ray and Charged Particle Detector," Proc. IEEE Nuclear Science Symposium, October 1966.

Table 1. Specifications.

Weight of gondola	4,000 pounds
Charge resolution	±0.15 charge
Top momentum (1 sigma)	±85 GV/c
Gondola shell	8 ft diam; average thickness, 3 mm
Total material in "beam"	6.9 g/cm^2
	0.12 interaction lengths
	0.42 radiation lengths
Spark chambers	Two pairs of modules 100 × 100 cm $\begin{bmatrix} \text{all with} \\ \text{1-cm gap} \\ \text{spacing} \end{bmatrix}$
	Two pairs of modules 80 × 80 cm
	10 kV applied to spark chambers
Detectors	Two: 40 × 40 × 3/8 inch Pilot Y (S_1, S_3)
	Two: 7 × 20 × 1/4 inch Pilot B (S_2R, S_2L)
	Two: 7 × 20 × 1/8 inch CsI(Na)(CsIR, CsIL)
	Two: 24-inch diam × 1/4 inch Pilot B (Anti R, Anti L)
Cameras	Two: 35-mm; 60,000 frame capacity
Dead time (for camera operation)	218 msec
Batteries	600 watts dissipated from
	Two: 200 amp-hour, 28-V packs and
	Two: 100 amp-hour, 28-V packs
Shielding	Weight: 10 pounds/shield for 2-inch photo-multiplier tube (10 inches long, 3-inch OD)
Optics	Demagnification, average factor of 62
	Real space resolution, 0.1 mm
Magnet	30-mil wire with 15-mil Nb-Ti core
	Short sample characteristics, 150 amp at 60 kG
	12,800 turns on coil

Table II. Trigger rates.

Threshold setting on S_1, S_2, and S_3	Anti status	Ungated rate (events/min)	Gated rate (events/min)
$Z \geq 1$	IN	2800	245
	OUT	4700	247
$Z \geq 2$	IN	590	186
	OUT	1830	239
$Z \geq 3$	IN	31	28
	OUT	245	130

FIGURE CAPTIONS

Fig. 1.   Assembled SSCM gondola.

Fig. 2.   SSCM differential geometry factor versus integral $\vec{B} \cdot \vec{dl}$.

Fig. 3.   Schematic SSCM detectors and cryogenics.

Fig. 4.   Electronics trigger logic.

Fig. 5.   Spark chamber pulser system.

Fig. 6.   Plot of the goodness of fit χ of four-spark helium segments
          straight line. Smooth curve shows the expected shape for
          a pure gaussian distribution with $\sigma = 0.14$ mm/spark.

Fig. 7.   Plot of straight-through (magnet OFF) events analyzed as
          curved tracks.

Fig. 8.   Histogram of average pulse heights of S_1, S_3, and CsI (R) anodes
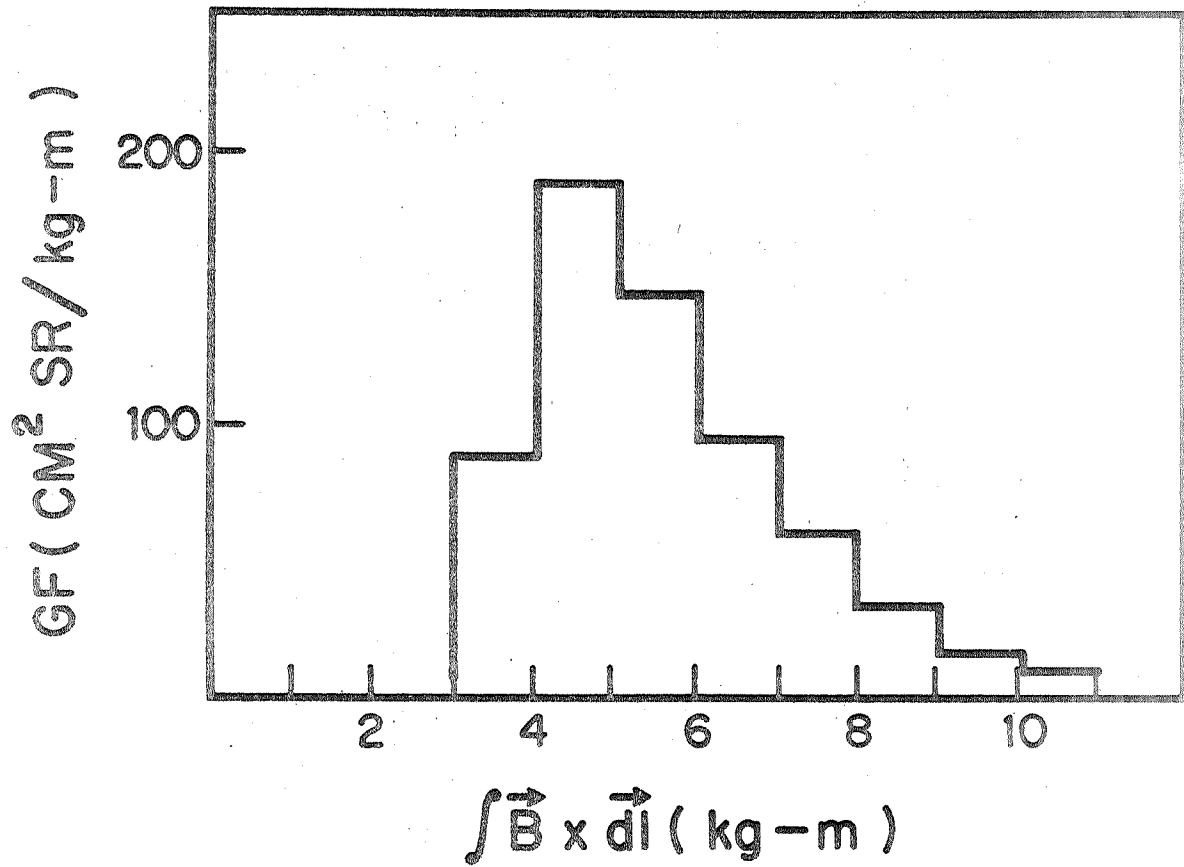   (722 events).

TOP SCINTILLATOR S1

MAGNET VENT
POLYURETHANE FOAM
SHELL .125 INCHES THICK

UPPER SPARK CHAMBERS
SUPERCONDUCTING MAGNET
LIQUID HELIUM RESERVOIR
PM TUBES
ANTI COINCIDENCE SCINT.
LOWER SPARK CHAMBERS

LOWER SCINTILLATOR S3

TRIGGER ELECTRONICS

BALLAST HOPPER –TWO

TELEMETRY, COMMAND
ELECTRONICS AND
BATTERY BOX

MIRROR ASSM.

PM TUBES

36 INCHES — 1 METER

0

SCALE

NCAR
BALLOON
CONTROL
ELECTRONICS

XBL 714-675

Fig. 1. L. H. Smith

Fig. 2. L. H. Smith

BOIL OFF RELIEF VALVES

PARTICLE TRAJECTORY

BOIL OFF STACK
BOIL OFF TUBE
CHARGE LEADS

S_1 TRIGGER COUNTER
40 X 40 INCHES

SPARK CHAMBERS
HELIUM FLASK
SUPERCONDUCTING MAGNET
OUTER VACUUM WALL
C_sI   7 X 20 INCHES

LIQUID HELIUM
RESERVOIR

HELIUM FLASK

S_2 TRIGGER COUNTER
7 X 20 INCHES

PERSISTENCY
SWITCH

ANTI COINCIDENCE COUNTER
24" DISC BOTH SIDES

CONNECTING TUBES

SPARK CHAMBERS

HELIUM TUBE

S_3 TRIGGER COUNTER
40 X 40 INCHES

1 METER

36 INCHES   0

SCALE

XBL 714-676

Fig. 3.   L. H. Smith

Fig. 4. L. H. Smith

"A" SYSTEM

"B" SYSTEM

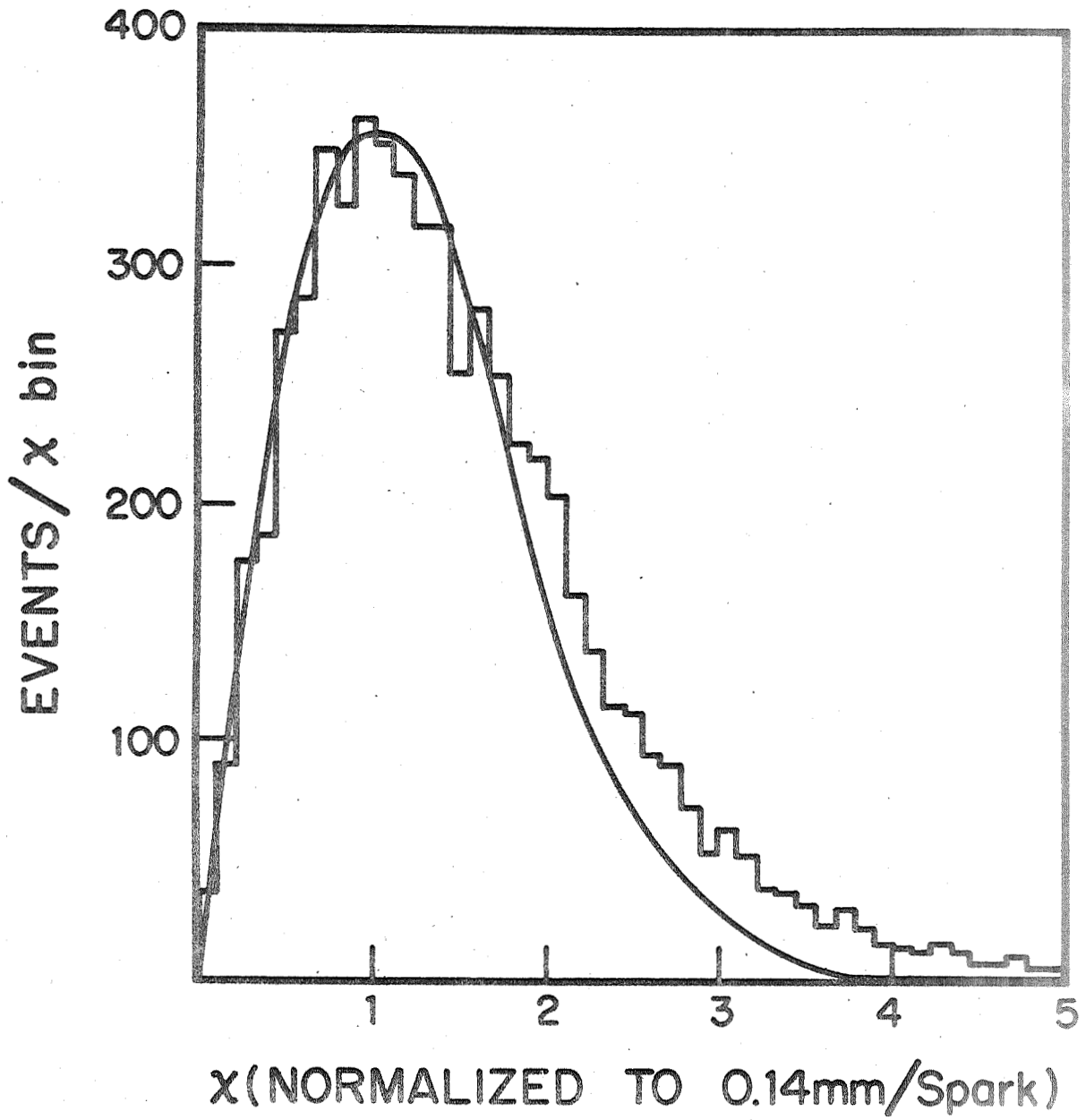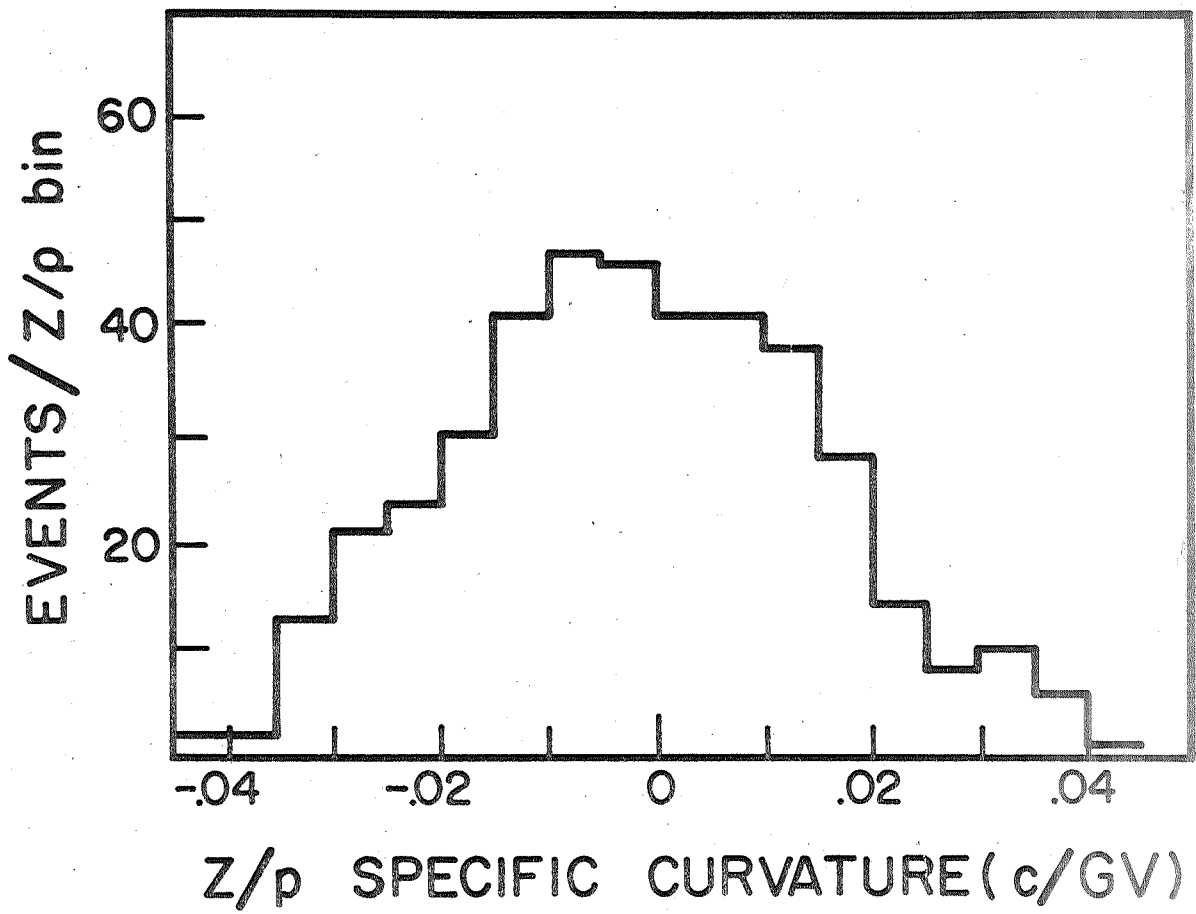SPARK CHAMBER MODULES

(FROM TRIGGER SYSTEM)
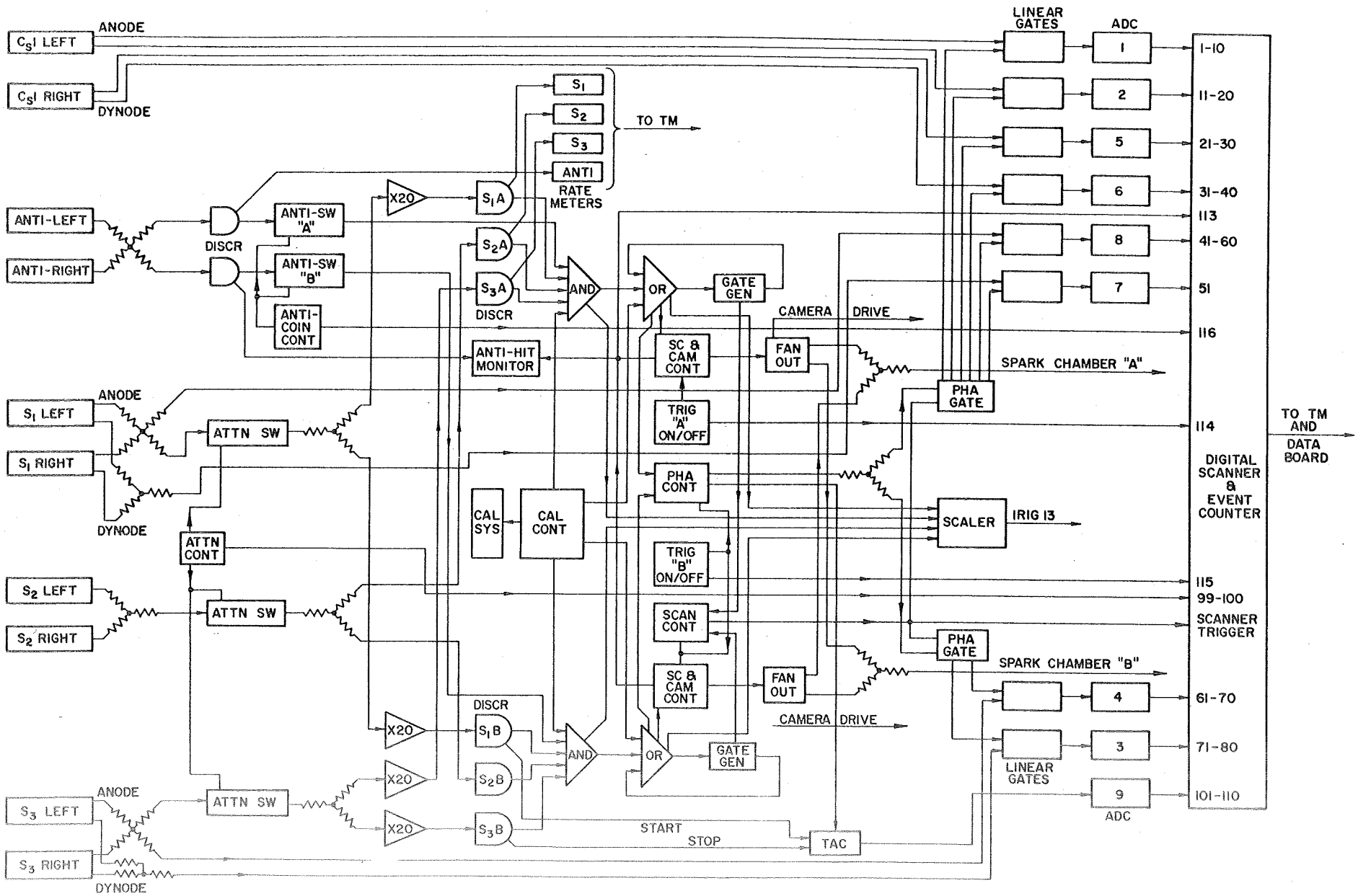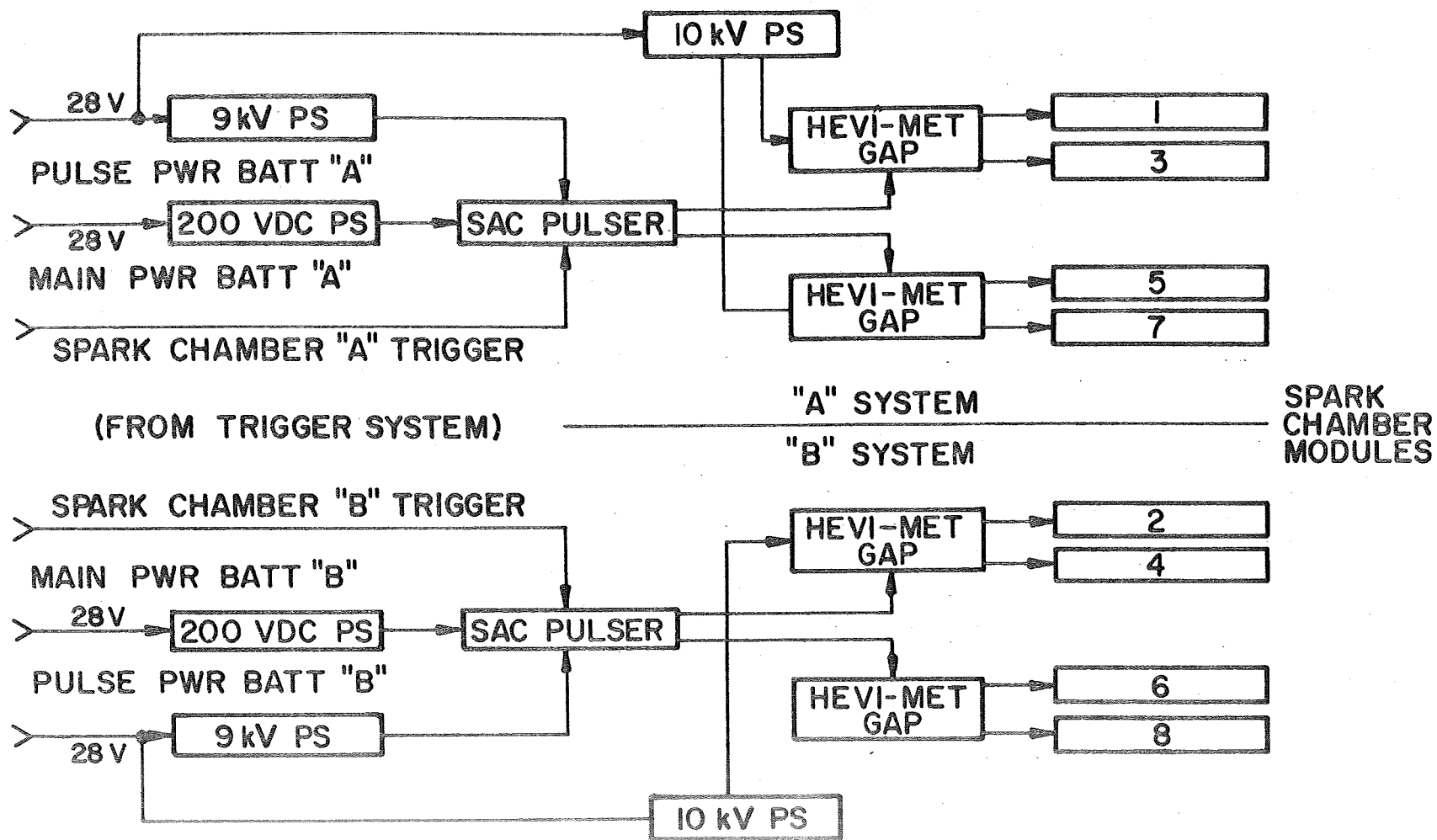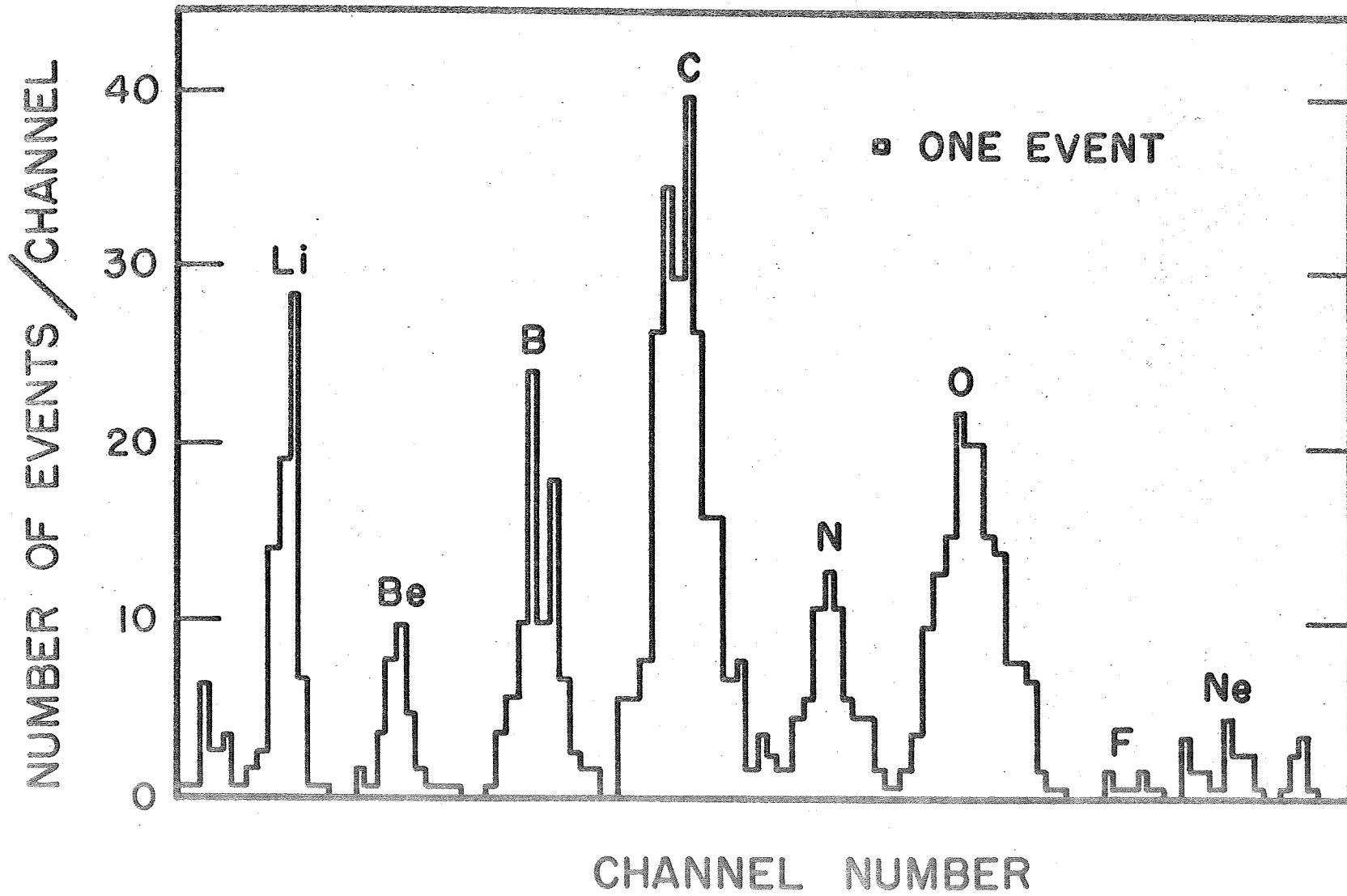
Fig. 5.   L. H. Smith

Fig. 6.   L. H. Smith

Fig. 7.   L. H. Smith

Fig. 8.   L. H. Smith